THE ASTROPHYSICAL JOURNAL, 338:152–161, 1989 March 1

IMPROVED ESTIMATES OF GALACTIC H II REGION EMISSION MEASURES AND FILLING FACTORS: LOW-FREQUENCY VLA OBSERVATIONS NEAR SHARPLESS 53

NAMIR E. KASSIM[1] AND KURT W. WEILER
E. O. Hulburt Center for Space Research, Naval Research Laboratory
WILLIAM C. ERICKSON
University of Maryland
AND
T. L. WILSON
Max-Planck-Institut für Radio Astronomie; and E. O. Hulburt Center for Space Research, Naval Research Laboratory
Received 1988 May 23; accepted 1988 August 10

ABSTRACT

VLA observations at 20 and 90 cm of five distant Galactic H II regions in an area including the Sharpless S53 complex have been used to measure their effective sizes and optically thick continuum flux densities. These data have been combined with shorter wavelength, optically thin flux density measurements and electron temperature estimates to determine accurate emission measures where previous results gave only lower limits. Our analysis indicates that existing lower limits to the emission measures often underestimate the true values by more than an order of magnitude.

Filling factors for the ionized gas in these H II regions have also been determined and values ranging from 0.03 to 0.50 indicate significant clumping. If these clumps are embedded in a lower density but more widely distributed ionized component, even our much higher emission measures are still lower limits to the true values for the clumps.

Subject headings: interferometry — nebulae: H II regions — nebulae: individual (Sharpless 53)

I. INTRODUCTION

Since early measurements by Mezger and Höglund (1967), radio continuum and recombination line observations have been used to estimate electron temperatures for Galactic H II regions (see Wilson 1980 and references therein). If an H II region is of uniform density, its local thermodynamic equilibrium (LTE) electron temperature (T_e) is directly related to the ratio of the measured recombination line (T_L) to continuum (T_C) brightness temperature. The value of T_e can then be combined with T_C to determine the emission measure (EM) of the region if the source is resolved by the telescope beam. If a region is either unresolved or significantly clumped, the EM determined in this way is only a lower limit.

Most early analyses were limited to assuming LTE and internal homogeneity to obtain a single value of T_e and EM for each H II region. However, over the last few years, efforts have concentrated on making detailed models of H II regions which include gradients in temperature and density as well as departures from LTE (Wilson and Jäger 1987). These models have generally been applied to well resolved, nearby H II regions such as the Orion Nebula where multifrequency observations are available. For more distant H II regions where such detailed observations are lacking, the assumptions of uniformity and LTE must still be made. Such oversimplifications can lead to artificially low EM values.

In this paper we use 90 cm continuum observations with the VLA[2] of five distant H II regions near the Sharpless 53 complex to obtain improved estimates of their physical properties. Specifically, we show that continuum observations at long wavelengths where the H II regions are optically thick can be used together with T_e values and flux density measurements obtained at shorter wavelengths where the regions are optically thin to determine accurate EM. We also show that such observations can be used to constrain the filling factors of the ionized gas in the H II regions.

II. OBSERVATIONS

Observations of the area around the H II complex S53 were obtained at 1480.7 MHz and 1536.2 MHz (λ20 cm, 12 antenna subarray) using 50 MHz bandwidth and at 327.5 MHz and 333.0 MHz (λ90 cm, 15 antenna subarray) using 3.0 MHz bandwidth during 1987 March in the "D" configuration (maximum baseline $\sim$1 km) of the VLA. The individual maps, after calibration, correction, and inspection for quality, were added to produce a single map for each observing band. These two "dirty" maps were then CLEANed and restored with elliptical Gaussians to an effective half-power beamwidth (HPBW) of 3.2 × 2.8 at position angle 25° at 90 cm and 1.6 × 0.9 at position angle −21° at 20 cm. The final maps, after correction for primary beam attenuation, are shown in Figures 1 (20 cm) and 2 (90 cm).

The total integration time for each map was approximately 1 hr and consisted of six 10 minute snapshots spread over an 8 hr period in order to maximize the available *uv* coverage. The measured rms noise level on the 20 cm map is $\sim$0.005 Jy beam^{-1}, and the corresponding figure on the 90 cm map is $\sim$0.05 Jy beam^{-1}.

Calibration at 20 cm used single 20 minute observations of primary calibrators 3C 286 and 3C 48, defined to have flux densities of 14.51 and 15.76 Jy, respectively, to determine the variable flux density of 1741−038, the secondary calibrator.

[1] National Research Council/NRL Cooperative Research Associate.
[2] The VLA (Very Large Array) is a facility of the National Radio Astronomy Observatory which is operated by Associated Universities, Inc. under contract to the National Science Foundation.

Report Documentation Page

Form Approved
OMB No. 0704-0188

1. REPORT DATE	2. REPORT TYPE	3. DATES COVERED
MAR 1989		**00-00-1989 to 00-00-1989**

4. TITLE AND SUBTITLE	5a. CONTRACT NUMBER
Improved Estimates of Galactic H pi Region Emission Measures and Filling Factors: Low-Frequency VLA Observations Near Sharpless 53	5b. GRANT NUMBER
	5c. PROGRAM ELEMENT NUMBER
6. AUTHOR(S)	5d. PROJECT NUMBER
	5e. TASK NUMBER
	5f. WORK UNIT NUMBER
7. PERFORMING ORGANIZATION NAME(S) AND ADDRESS(ES) **Naval Research Laboratory,Code 7213,4555 Overlook Avenue, SW,Washington,DC,20375**	8. PERFORMING ORGANIZATION REPORT NUMBER
9. SPONSORING/MONITORING AGENCY NAME(S) AND ADDRESS(ES)	10. SPONSOR/MONITOR'S ACRONYM(S)
	11. SPONSOR/MONITOR'S REPORT NUMBER(S)

12. DISTRIBUTION/AVAILABILITY STATEMENT
Approved for public release; distribution unlimited

13. SUPPLEMENTARY NOTES

14. ABSTRACT

15. SUBJECT TERMS

16. SECURITY CLASSIFICATION OF:			17. LIMITATION OF ABSTRACT	18. NUMBER OF PAGES	19a. NAME OF RESPONSIBLE PERSON
a. REPORT **unclassified**	b. ABSTRACT **unclassified**	c. THIS PAGE **unclassified**		**10**	

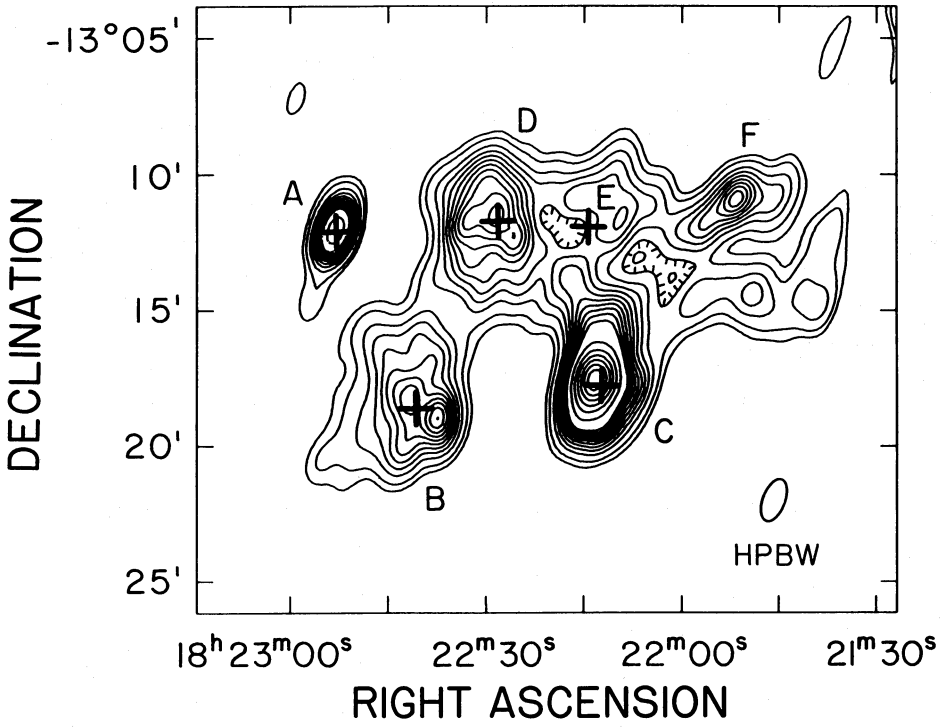

FIG. 1.—Final contour map at 20 cm of the region around the H II complex S53. Five distinguishable H II regions are arbitrarily labeled A–E, and an adjacent nonthermal source (see text) is labeled F. The positions of H110α detections (Downes *et al.* 1980) are marked with plus signs. Contour levels are (0.5, 1, 2, 3, ..., 10, 15, 20, 25, ...) × 0.05 Jy beam^{-1} with a peak brightness of 2.2 Jy beam^{-1} at source C. An ellipse illustrating the synthesized half-power beam width (HPBW) is shown in the lower right-hand corner.

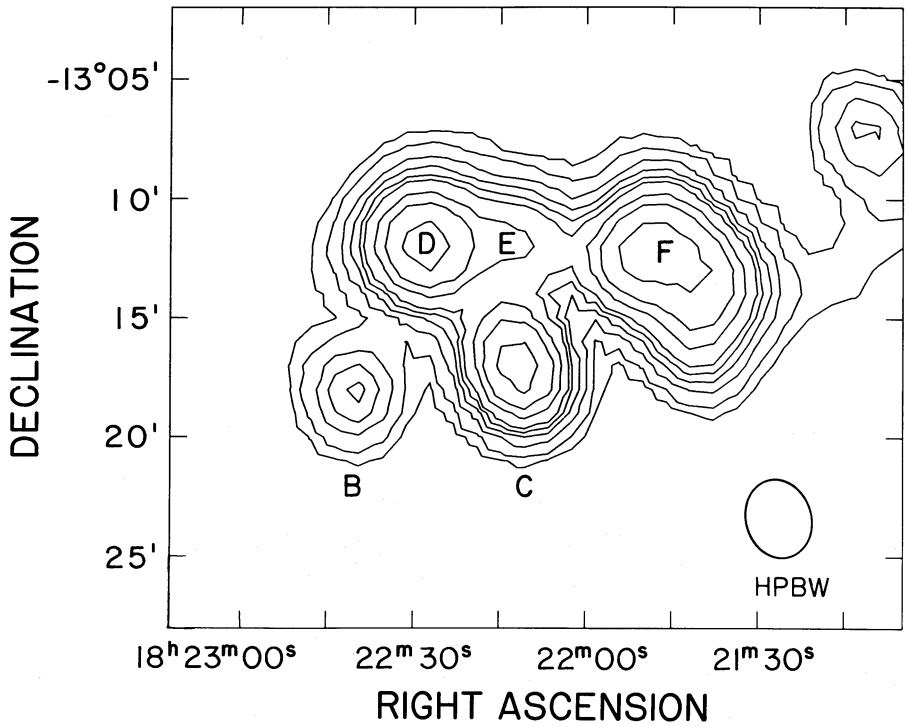

FIG. 2.—Final contour map at 90 cm of the region around the H II complex S53. The distinguishable sources (B–F) are labeled as in Fig. 1 with source A no longer detectable at this frequency. The source at the right-hand edge of the map near $\alpha = 18^h21^m10^s$, $\delta = -13°07'$ is apparently nonthermal and is thought to be unrelated to the complex. The contour levels are (1, 2, 4, 6, 8, 10, 15, 20, 30, 40, ...) × 0.05 Jy beam^{-1} with a peak brightness of 2.0 Jy beam^{-1} at source F. An ellipse illustrating the synthesized half-power beam width (HPBW) is shown in the lower right-hand corner.

Observations for ~10 minutes each hour of 1741−038 then were used to fix the phase corrections and flux density scale for the 20 cm data set. At 90 cm no secondary calibrators were used, and flux density and phase calibration were based on observations of 3C 286, 3C 380, and 3C 48, which were defined to have flux densities of 29 Jy, 45 Jy, and 47 Jy, respectively. Standard computer programs were used to interpolate the gain and phase of the instrument between calibrator observations. These procedures are normal for the VLA and are thought to provide a phase and flux density calibration which is consistent to a few percent with possible systematic errors of up to ~5% at both wavelengths. For a more detailed description of the VLA see Napier, Thompson, and Ekers (1983).

The shortest array spacings at 20 cm and 90 cm were ~200λ and ~ 55λ, respectively. This means that sources larger than ~3′ at 20 cm and ~10′ at 90 cm may be undersampled and have their flux densities underestimated by >~10%. However, since our individual sources are all <~4′ in size (except source E which is ~7′ in one dimension), this is not a problem, especially not for the more critical 90 cm flux densities. Evidence for the accurate detection of large-scale structure is also given by the fortuitous presence of the extended SNR G18.8 + 0.3 within the 90 cm field of view. This source is much larger than sources A–E and is comparable in size (~25′) to the whole S53 complex. Its radio spectrum is well determined from centimeter to dekametric wavelengths (see Kassim 1987) and our 90 cm integrated flux density of 37 Jy is only ~25% lower than the expected 50 Jy. This is well within the ~50% error to which the 90 cm flux density can be predicted from the known spectrum.

A difficulty with 90 cm observations at the VLA is crosstalk between antennas of the array. This is particularly severe in the "D" configuration for low-declination sources, when the antennas are pointed nearly towards the backs of their neighbors, and can lead to large, low-frequency "ripples" across the maps. Intensive investigation of the problem and consultation with other observers showed that such ripples could be minimized by eliminating many of the short baselines in the observations. In our case, this was found to mainly affect telescopes on the southeast arm of the VLA, and the shortest baselines on this arm had to be eliminated from the data set. Even though the maps still do not reach the theoretical random noise of ~0.002 Jy beam^{-1} expected for the 90 cm observations, no other data editing or correcting procedures could be found to further improve the results. As time and money permit, shielding is being installed on individual telescopes at the VLA to reduce or eliminate this problem. In the meantime, our editing reduced the effects to manageable levels while still permitting the retention of enough short 90 cm baselines to retain large scale structure information in the maps.

III. RESULTS

The 20 cm map (Fig. 1) reveals six discrete sources which have been arbitrarily labeled A–F for reference. Plus signs show the positions where the 6 cm H110α recombination line emission has been found (Downes *et al.* 1980) thus identifying sources A–E as H II regions. Source F shows no H110α emission and also has a steep spectrum (see below) so that it is almost certainly nonthermal.

The parameters for the H110α line observations are listed in the upper part of Table 1. They include measurements of the brightness temperature in the continuum and in the line, the velocity of the line, and estimates of EM and T_e calculated by assuming the sources are optically thin and in LTE. These estimates of EM are lower limits for sources unresolved by the 2.′7 beam of the Effelsberg 100 m telescope or for sources with significant clumping. For sources A and C the parameters (except for the EM) are also given in the lower part of Table 1 from the Effelsberg H76α recombination line survey by Wink, Wilson, and Bieging 1983 (resolution ~1′). These T_e estimates are thought to be less sensitive to non–LTE effects. In any case, they do not differ from those determined from the H110α line observations by more than ~30% which is in agreement with the finding that LTE electron temperatures are frequently close to actual T_e (see, e.g., Wilson 1980).

Sources B–E have line velocities which are all within 6.5 km s^{-1} of each other. Based on complimentary H_2CO absorption measurements (and earlier H I observations), Downes *et al.*

TABLE 1

RECOMBINATION LINE MEASUREMENTS NEAR S53

A. RESULTS FROM H110α OBSERVATIONS (Downes *et al.* 1980)

Source	R.A. (1950)	Decl. (1950)	Continuum Temperature[a] T_C (K)	Line Temperature[a] T_L (K)	Velocity (km s^{-1})	Emission Measure EM (cm^{-6} pc)	Electron Temperature[b] T_e (K)
A.....	18^{h}22^{m}53^s	−13°12′00″	3.2	0.15	32.3	3.2×10^5	7300
B.....	18 22 41	−13 18 31	3.2	0.34	45.5	4.4×10^4	6200
C.....	18 22 12	−13 17 41	9.5	0.68	52.0	5.9×10^5	5800
D.....	18 22 28	−13 11 50	4.0	0.20	47.5	4.4×10^4	5300
E.....	18 22 15	−13 12 02	3.2	0.17	47.0	2.9×10^4	7600

B. RESULTS FROM H76α OBSERVATIONS (Wink *et al.* 1983)

Source	R.A. (1950)	Decl. (1950)	Line-to-Continuum Ratio T_L/T_C	Velocity (km s^{-1})	Electron Temperature T_e (K)
A.....	18^{h}22^{m}53^s	−13°12′00″	0.232 ± 0.019	33.7 ± 1.3	5100 ± 600
C.....	18 22 12	−13 17 41	0.240 ± 0.022	53.0 ± 1.3	6300 ± 700

[a] Brightness temperature = antenna temperature/0.65.

[b] The errors in the electron temperatures are estimated by Downes *et al.* 1980 to be ±2500 K.

TABLE 2

VLA RESULTS FOR SOURCES NEAR S53

			90 CENTIMETERS		20 CENTIMETERS			
SOURCE (1)	R.A. (1950)[a] (2)	DECL. (1950)[a] (3)	Peak Brightness (Jy beam^{-1}) (4)	Integrated Flux Density $S_{90\,cm}$ (Jy) (5)	Peak Brightness (Jy beam^{-1}) (6)	Integrated Flux Density $S_{20\,cm}$ (Jy) (7)	SPECTRAL INDEX[b] α (90–20 cm) (8)	SIZE[c] (9)
A.....	$18^h22^m53^s$	−13°12′00″	≤0.05	...	0.97	1.07 ± 0.05	> +2.0	≤0.′7
B.....	18 22 37	−13 19 00	0.48	0.61 ± 0.20	0.50	3.20 ± 0.40	+1.1	4.4 × 2.8
C.....	18 22 13	−13 17 40	1.85	2.61 ± 0.20	2.22	6.30 ± 0.80	+0.6	2.4 × 1.3
D.....	18 22 29	−13 11 30	1.40	1.84 ± 0.06	0.53	4.07 ± 0.90	+0.5	4.2 × 3.3
E.....	18 22 09	−13 11 40	0.78	2.77 ± 0.11	0.27	>1.80	> −0.3	7.5 × 3.3
F.....	18 21 52	−13 10 49	2.00	5.69 ± 0.27	0.44	1.24 ± 0.28	−1.0	3.6 × 0.8

[a] Positions are obtained from the 20 cm map.

[b] $S \propto \nu^{+\alpha}$.

[c] Sizes are estimated from the 20 cm map (Fig. 1) expect for source E which, because of its large size and low surface brightness, was best estimated from the 90 cm map.

(1980) conclude that sources B–E are all at the near kinematic distance of ~4.5 kpc. We therefore accept these sources as being physically associated with the S53 complex since the brightest source C is coincident with the H II region Sharpless S53 (Sharpless 1959). However, the analysis which follows is independent of any physical association between the sources. Source A also appears to be an H II region but, because of its large velocity difference, is presumably not physically associated with the S53 complex.

Table 2 summarizes the results from our VLA maps. Source sizes were obtained from the higher resolution 20 cm map except for source E whose large size was better estimated from the 90 cm map. Comparison of Figure 1 with Figure 2 shows that source A is undetected at 90 cm, presumably because of self-absorption.

Source F is stronger at 90 cm than at 20 cm and has a nonthermal spectrum. Odegard (1986) has suggested, on the basis of 57.5 MHz observations made at the Clark Lake Radio Observatory (Erickson, Mahoney, and Erb 1982), that it is a previously unidentified Galactic supernova remnant (G18.1 − 0.2). It could thus be associated with S53 but since we are only concerned here with determining H II region properties, we do not discuss it further.

Integrated flux densities are also listed in Table 2. These were obtained by averaging a fitted Gaussian model value and a direct contour map integration value with errors conservatively defined to be the difference between the two determinations. In all cases these error estimates exceed those expected due to random noise.

Figure 3 shows an overlay of our 20 cm VLA map (Fig. 1)

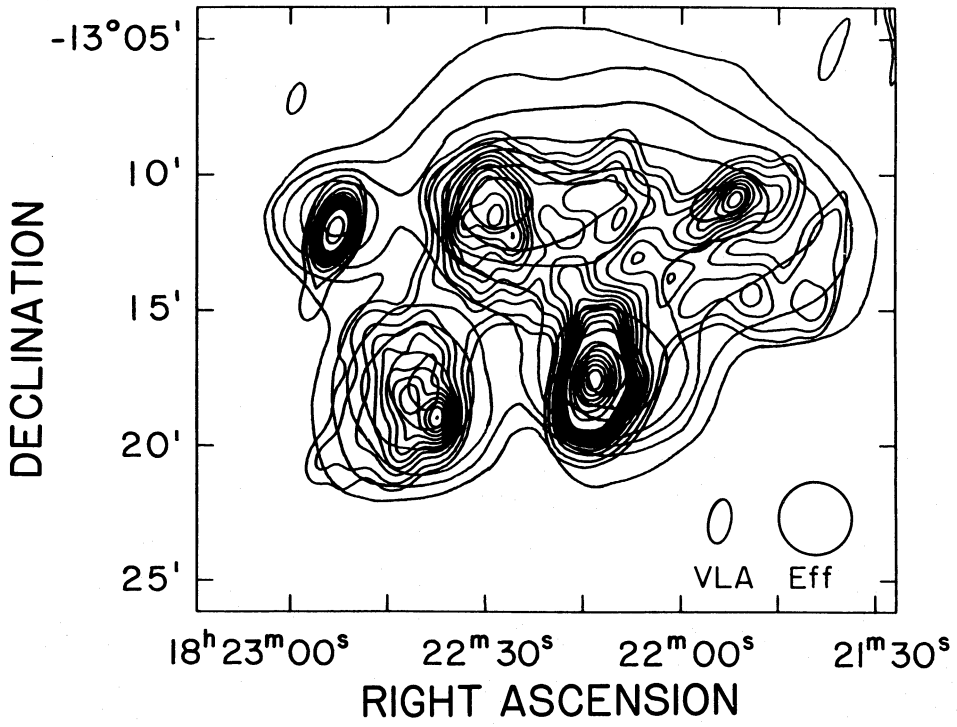

FIG. 3.—Overlay of the 6 cm single-dish continuum map of Altenhoff *et al.* (1978) with our 20 cm VLA map shown in Fig. 1. The half-power beam widths for the VLA and the Effelsberg 100 m telescope are illustrated in the lower right-hand corner.

TABLE 3

FLUX DENSITIES FOR H II REGIONS NEAR S53 FROM CENTIMETER WAVELENGTH CONTINUUM OBSERVATIONS

Source	Wavelength (cm)	Peak Brightness (Jy beam^{-1})	Integrated Flux Density S (Jy)	References
A.....	11	...	0.93 ± 0.56	1
	6	1.35	1.50 ± 0.18	2
	3	...	1.40 ± 0.36[a]	3
B.....	11	...	1.86 ± 0.56	1
	6	1.36	2.90 ± 0.30	2
C.....	11	...	5.28 ± 0.56	1
	6	4.70	5.50 ± 0.18	2
	3	4.22	4.75 ± 0.36	3
D.....	11	...	3.35 ± 0.56	1
	6	1.70	5.10 ± 0.34	2
E.....	6	1.60	8.80 ± 0.60	2

[a] Estimated from the Handa *et al.* 1988 map assuming that source A is unresolved by their observing beam.

REFERENCES.—(1) Reich *et al.* 1984; (2) Altenhoff *et al.* 1978; (3) Handa *et al.* 1988.

with the 6 cm, single-dish continuum map of Altenhoff *et al.* (1978). The Altenhoff *et al.* map was made with a beamwidth of ~2.'7. As expected, all of the flat spectrum, thermal sources A-E clearly appear on the 6 cm map while the steeper spectrum, nonthermal source F becomes less prominent. The 11 cm (resolution ~4.'3; Reich *et al.* 1984) and 3 cm (resolution ~3.'0; Handa *et al.* 1988) single-dish Galactic plane surveys show very similar structure for the area. Where possible, integrated flux densities for each of the five thermal sources A–E have been collected in Table 3 from these single-dish surveys. These values are taken from the published source lists in the original references so that not all sources have listed flux densities at all frequencies.

Errors for the integrated flux densities listed in Table 3 are difficult to obtain since estimates are generally not given in the published source lists. Therefore, we assume that the principal source of error arises in the difficulty of estimating the local background levels on the survey maps and, somewhat arbitrarily, we assign an error of one-half of the assumed local background brightness. This is very conservative since background levels have probably been determined more accurately than this in each of the three surveys.

IV. DISCUSSION

The radio flux density of a spherical H II region in the LTE, homogeneous nebula approximation (Hjellming, Andrews, and Sejnowski 1969) is given by

$$S = 3.07 \times 10^{-2} T_e \nu^2 \Omega (1 - e^{-\tau}) , \quad (1)$$

where S is the integrated flux density in Jy, T_e is the electron temperature in Kelvin, ν is the observing frequency in MHz, Ω is the solid angle subtended by the source in steradians, and τ is the optical depth. At radio wavelengths τ is given (Mezger and Henderson 1967) approximately by

$$\tau \sim 1.643 \times 10^5 \nu^{-2.1} \text{ EM } T_e^{-1.35} , \quad (2)$$

where EM is the emission measure in cm^{-6} pc, defined as

$$\text{EM} = \int_L n_e^2 \, dl \quad (3)$$

with n_e the thermal electron density in cm^{-3} and l the path length in parsecs along a line of sight L through the source.

In the optically thin limit of very low opacity ($\tau \ll 1$; $1 - e^{-\tau} \sim \tau$) equations (1) and (2) reduce to

$$S = 3.07 \times 10^{-2} T_e \nu^2 \Omega \tau = 5 \times 10^3 T_e^{-0.35} \nu^{-0.1} \Omega \text{ EM} \quad (4)$$

and in the optically thick limit of very high opacity ($\tau \gg 1$; $1 - e^{-\tau} \sim 1$) equations (1) and (2) give

$$S = 3.07 \times 10^{-2} T_e \nu^2 \Omega . \quad (5)$$

The short-wavelength–determined T_e, EM, and S values presented in Tables 1 and 3 combined with equations (1) and (2), in principle, entirely determine the spectra for the five H II regions A–E if the sources are uniform and the filling factors are known. In practice, effective source sizes (filling factors) are poorly determined and the EM obtained from recombination line measurements are only lower limits. However, since our 90 cm measurements (Table 2) are in the optically thick portion of the spectrum of the H II regions, we can now constrain the source parameters far better than previously possible.

First, let us consider the previously available, short-wavelength–determined information. Assuming that all sources are optically thin at 11, 6, and 3 cm (an approximation which is justified by estimates of τ from eq. [2]), equation (4) can be solved for the effective source size as

$$\Omega = 5 \times 10^{-4} S_{3\,\text{cm}} T_e^{0.35} \text{ EM}^{-1} , \quad (6)$$

where $S_{3\,\text{cm}}$ is the 3 cm flux density in Jy. Our 20 cm VLA flux density values are not used since that wavelength lies in an intermediate range where the $\tau \ll 1$ approximation may not be valid. To obtain an accurate $S_{3\,\text{cm}}$ and minimize the problems in determining baseline levels inherent in single-dish Galactic surveys, we fit a $S \propto \nu^{-0.1}$ spectrum to all 11, 6, and 3 cm measurements available (Table 3) for each H II region, weighting all wavelengths equally. These "best" values for $S_{3\,\text{cm}}$ obtained from the fit (Table 4, col. [2]), together with T_e and EM from Table 1 (repeated in Table 4, Cols. [3] and [4] for convenience), were then used in equation (6) to calculate short wavelength effective source sizes $\Omega_{S\lambda}$ (Table 4, col. [5]). From these short-wavelength results alone, an entire spectrum for each H II region, including the optically thick part, is now determined. Substituting the values from Table 4 into equations (1) and (2) yields the dashed curves shown in Figures

TABLE 4

PARAMETERS DETERMINED FROM SHORT-WAVELENGTH (OPTICALLY THIN) RADIO MEASUREMENTS

Source (1)	$S_{3\,\text{cm}}$[a] (Jy) (2)	T_e[b] (K) (3)	EM[b] (cm^{-6} pc) (4)	Effective Source Size $\Omega_{S\lambda}$ (sr) (5)
A.....	1.21	5100	3.2×10^5	3.7×10^{-8}
B.....	2.17	6200	4.4×10^4	5.2×10^{-7}
C.....	4.84	6300	5.9×10^5	8.7×10^{-8}
D.....	3.85	5300	4.4×10^4	8.8×10^{-7}
E.....	8.21	7600	2.9×10^4	3.2×10^{-6}

[a] Estimated by fitting an $\alpha = -0.1$ spectrum to the 11, 6, and 3 cm values (when available) from short-wavelength surveys.

[b] Obtained from recombination line measurements (Table 1).

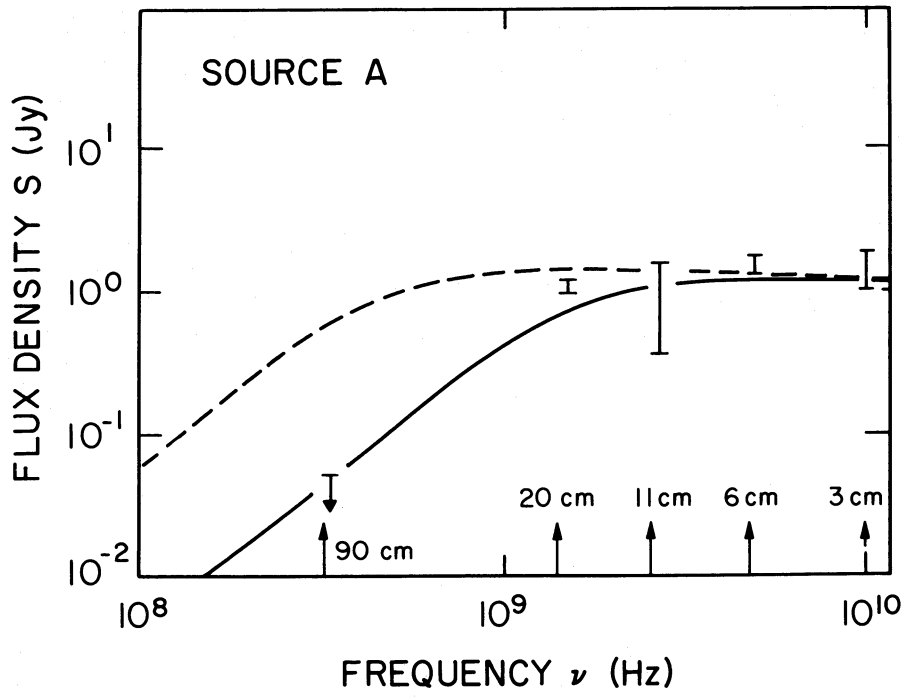

FIG. 4*a*

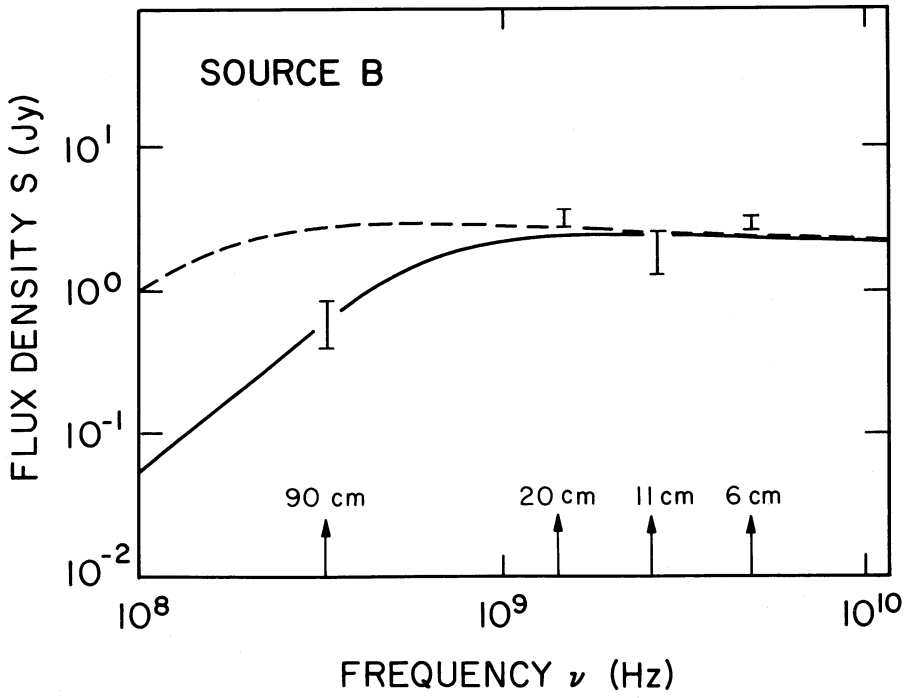

FIG. 4*b*

FIG. 4.—Radio spectra for the five H II regions A–E (see Fig. 1) near the S53 complex. Data points are taken from Tables 2 and 3 with the best estimates for their appropriate errors shown. The dashed curves are the spectra expected if the source parameters are entirely determined by existing short wavelength observations. The solid curves are those obtained if the parameters of the H II regions are refined through use of our 90 cm VLA observations. As is clear, the calculated spectrum's fit to the data, and therefore the physical description of the regions, is greatly improved by our new data.

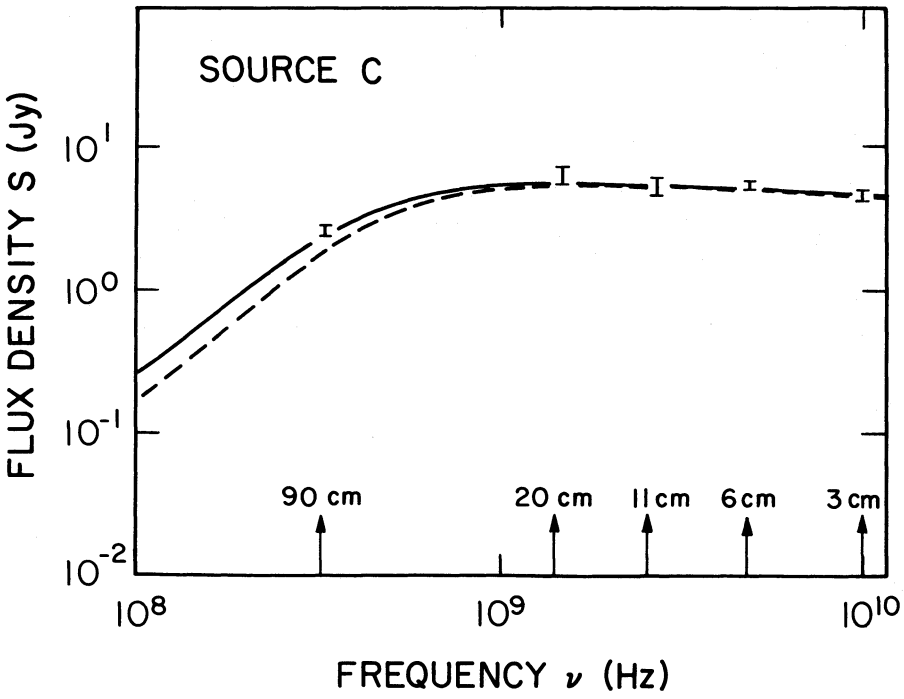

FIG. 4*c*

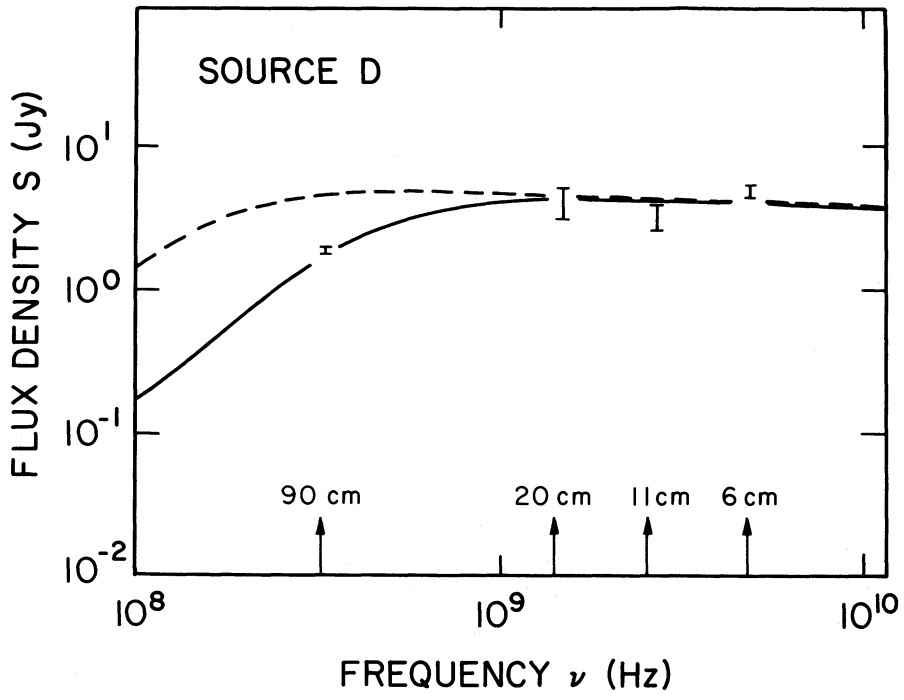

FIG. 4*d*

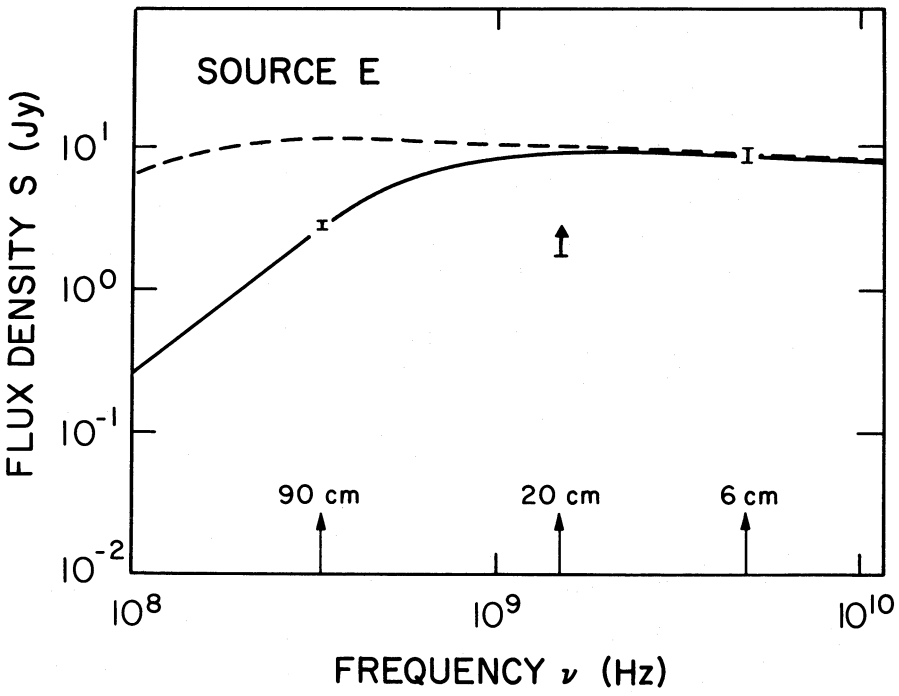

FIG. 4e

4a–4e. On these figures we have also plotted all flux densities available between 90 cm and 3 cm for each of the H II regions (from Tables 2 and 3) including estimates (see preceding section) of their errors.

It is clear from Figures 4a–4e that, except for source C, existing (short-wavelength–determined) parameters predict continuum flux densities at 90 cm which are at least an order of magnitude larger than those actually observed. Such discrepancies can be explained in two ways: (1) our 90 cm flux densities are substantially underestimated, or (2) the model parameters determined from only the short-wavelength measurements are significantly in error. The former is unlikely (see § II), so let us consider the latter.

Any error in the models must lie in the parameters Ω, T_e, and/or EM determined from the short wavelength measurements alone, or in the value of $S_{3\,\mathrm{cm}}$. Also, any error must be very large since the predicted (Figs. 4a–4e, *dashed lines*) and measured 90 cm flux densities generally differ by more than an order of magnitude.

The value of $S_{3\,\mathrm{cm}}$ is unlikely to be in error by as much as 50% and is almost certainly not the origin of the order-of-magnitude discrepancies we find. Errors in its measurement come mainly from uncertainties in determining background levels associated with the extended Galactic nonthermal emission. However, our "best" estimates for $S_{3\,\mathrm{cm}}$, obtained from the fitting procedure described above, are quite consistent with slightly longer wavelength values and with direct measurements (when available) at 3 cm (Handa *et al.* 1988).

Values for T_e obtained from the H110α recombination line observations (Table 1) assume LTE but have typical quoted errors of only ~10%–40%. Moreover, results of the H76α line survey (which is relatively insensitive to non–LTE effects) available for sources A and C (see Table 1) compared with those of the H110α survey show that departures from LTE electron temperatures are not more than ~30%. That LTE values for T_e are approximately correct has more generally been found to be the case (see, e.g., Wilson 1980) and is to be expected since the non–LTE effects of stimulated emission and of pressure broadening tend to cancel each other (Seaton 1980). Also, non–LTE effects tend to *underestimate* the true T_e which would *increase* the discrepancy between the measured and predicted values of $S_{90\,\mathrm{cm}}$ rather than decrease it.

It appears, therefore, that the large differences between model predictions and measurements must arise in the short-wavelength estimates of EM and their interplay with effective source sizes (eq. [6]). This is not unexpected since estimates of EM from recombination line observations are known to be lower limits.

Accepting T_e, $S_{90\,\mathrm{cm}}$, and $S_{3\,\mathrm{cm}}$ as relatively well determined and sources A-E as optically thin ($\tau \ll 1$) at 3 cm and optically thick ($\tau > 1$) at 90 cm, by assuming that the effective source size has no frequency dependence ($\Omega_{90\,\mathrm{cm}} = \Omega_{3\,\mathrm{cm}}$) (the validity and effects of this assumption are discussed below), we can solve equations (4) and (5) to give

$$\mathrm{EM} = 1.65 T_e^{1.35} S_{3\,\mathrm{cm}} S_{90\,\mathrm{cm}}^{-1} . \quad (7)$$

These new estimates for the EM are listed in Table 5, column (2).

Figures 4a–4e show the spectra calculated from models where the EM values from Table 5 have been used (*solid curves*). As they must, these curves pass through the "best" $S_{3\,\mathrm{cm}}$ and the measured $S_{90\,\mathrm{cm}}$ values. They also describe well our intermediate frequency $S_{20\,\mathrm{cm}}$ values and the short-wavelength, optically thin flux density points from the literature. It should be noted that these new EM (Table 5, col [2]) are significantly different from the previously available estimates (Table 4, col. [4]).

Physically, determining EM based on T_e, $S_{90\,\mathrm{cm}}$, and $S_{3\,\mathrm{cm}}$ (eq. [7]) means that we have determined an effective source size Ω from $S_{90\,\mathrm{cm}}$ and T_e rather than from measurements in the

TABLE 5

NEW PARAMETER ESTIMATES FOR SOURCES NEAR S53

Source	EM[a] (cm^{-6} pc)	$\Omega_{90\ cm}$[b] (sr)	Ω_{map}[c] (sr)	Filling Factor $\Omega_{90\ cm}/\Omega_{map}$
A.....	4.2×10^6	$\leq 3.0 \times 10^{-9}$	$\leq 4.6 \times 10^{-8}$	0.07
B.....	8.0×10^5	3.0×10^{-8}	1.1×10^{-6}	0.03
C.....	4.2×10^5	1.3×10^{-7}	2.6×10^{-7}	0.50
D.....	3.8×10^5	1.1×10^{-7}	1.2×10^{-6}	0.09
E.....	8.7×10^5	1.1×10^{-7}	2.1×10^{-6}	0.05

[a] Calculated with eq. (7) by using our new 90 cm integrated flux density measurements ($S_{90\ cm}$; Table 2, col. [5]), our "best" estimated 3 cm flux density measurements ($S_{3\ cm}$; Table 4, col. [2]), recombination line derived electron temperatures (T_e; Table 4, col. [3]), and by assuming that the sources are optically thin ($\tau \ll 1$) at 3 cm, optically thick ($\tau > 1$) at 90 cm, and have effective source sizes which are frequency-independent ($\Omega_{3\ cm} = \Omega_{90\ cm}$).

[b] Calculated with eq. (5) using $S_{90\ cm}$ and recombination-line–derived T_e.

[c] Calculated from measured sizes given in Table 2, col. (9); see note c to Table 2.

optically thin portion of the radio spectrum as we did previously with equation (6). It is useful, therefore, to calculate these new values of $\Omega_{90\ cm}$ (Table 5, col. [3]) and compare them with our previous short wavelength determined estimates ($\Omega_{S\lambda}$; Table 4, col. [5]) and with direct measurements of apparent source sizes on our 20 cm map, Figure 1 (Ω_{map}; Table 5, col. [4]).

First, it is apparent that the measured 20 cm sizes (Ω_{map}) are the largest, or almost the largest, in all cases. This is to be expected since the Ω in our equations is not strictly the size subtended by the source but is an effective size which includes a filling factor. Second, the source sizes calculated from short-wavelength measurements ($\Omega_{S\lambda}$) are inversely proportional to the estimated short wavelength EM which we have shown to be grossly underestimated. This leads to size estimates which are consistently too large except for source C where the short-wavelength estimate appears to already give a reasonable value.

The best estimates for effective source sizes are $\Omega_{90\ cm}$ from our observations. These can be used to obtain source filling factors by taking their ratio to the apparent physical source sizes Ω_{map}. This ratio is given in Table 5, column (5). (Note that these filling factors are only limits in cases where the source is unresolved at 20 cm; i.e., for source A.)

The filling factors in Table 5 range from 0.03 to 0.50 and indicate that significant clumping is present in all sources. How does this affect our basic assumption that the gas which we see in the optically thin regime is the same as that which we see in the optically thick regime—i.e., that $\Omega_{90\ cm} = \Omega_{3\ cm}$? Let us consider the worst case of an H II region consisting of high-density clumps embedded in a lower density extended medium such as a raisin pudding model.

At first examination such a scenario would appear to cause difficulties. At shorter wavelengths where both components are optically thin most of the emission arises from the gas with the highest EM, i.e., from the clumps, while at the longer wavelengths the clumps become optically thick first and emission from the diffuse component dominates. Such considerations imply that source sizes determined from long wavelength measurements should tend to *overestimate* Ω for the clumps. However, comparison of $\Omega_{90\ cm}$ (Table 5, col. [3]) with $\Omega_{S\lambda}$ (Table 4, col. [5]) shows that to clearly not be the case. This also implies that the diffuse gas (the pudding), if present, is still optically thin at 90 cm.

Although the possibility exists that our new estimates are only lower limits to the EM and upper limits to the effective source sizes, they appear to be the best values currently available for H II regions near the S53 complex.

V. CONCLUSIONS

We have used 20 and 90 cm VLA observations of five H II regions, four of which may be physically associated with the S53 complex, to measure their continuum flux densities and apparent angular sizes. We have then combined these data with electron temperatures and flux densities determined from centimeter wavelength recombination line and continuum observations to obtain improved estimates of the emission measures and filling factors for each of the H II regions.

Previously available emission measure estimates have been shown to often be gross underestimates by an order of magnitude or more. Effective source sizes determined by our 90 cm observations compared with apparent source sizes on our 20 cm map show that the filling factors for these H II regions range from $\sim$0.03 to 0.5 and indicate that the gas is significantly clumped.

Our new results, combined with source modeling, provide greatly improved estimates of H II region physical parameters and allow accurate prediction of their radio spectra over more than 15 octaves.

VI. SUGGESTIONS FOR FUTURE WORK

The question of clumping in H II regions is important since it affects all parameter estimates. To investigate this further, we recommend that a search be made for low-frequency recombination lines from the S53 complex. These lines are produced by stimulated emission and cannot be emitted from high-density gas because of opacity and pressure broadening. Therefore, they become an ideal probe for the presence of any low-density, distributed gas (the pudding around the raisins). Also, ideal conditions are present for production of these lines in the direction of S53 because the presence of strong, nonthermal background emission from the inner Galactic plane can enhance stimulated emission.

That low-frequency recombination line observations should enable the construction of more detailed models of clumpy H II complexes is not a new idea (see Anantharamaiah 1986 and references therein), but little work has so far been done. Partly this is due to the fact that instruments with sufficient resolution for low-frequency spectral line studies of individual sources have only recently become available.

REFERENCES

Altenhoff, W. J., Downes, D., Pauls, T., and Schraml, J. 1978, *Astr. Ap. Suppl.*, **35**, 23.

Anantharamaiah, K. R. 1986, *J. Ap. Astr.*, **7**, 131.

Downes, D., Wilson, T. L., Bieging, J., and Wink, J. 1980, *Astr. Ap. Suppl.*, **40**, 379.

Erickson, W. C., Mahoney, M. J., and Erb, K. 1982, *Ap. J. Suppl.*, **50**, 403.

Handa, T., Sofue, Y., Nakai, N., Hirabayashi, H., and Inoue, M. 1988, *Pub. Astr. Soc. Jap.*, **39**, 709.

Hjellming, R. M., Andrews, M. H., and Sejnowski, T. J. 1969, *Ap. J.*, **157**, 573.

Kassim, N. E. 1987, Ph.D. thesis, University of Maryland.

Mezger, P. G., and Henderson, A. P. 1967, *Ap. J.*, **147**, 471.

Mezger, P. G., and Höglund, B. 1967, *Ap. J.*, **147**, 490.

Napier, P. J., Thompson, A. R., and Ekers, R. D. 1983, *Proc. IEEE*, **71**, 1295.
Odegard, N. 1986, *A.J.*, **92**, 1372.
Reich, W., Fürst, E., Steffen, P., Reif, K., and Haslam, C. G. T. 1984, *Astr. Ap. Suppl.*, **58**, 197.
Seaton, M. J. 1980, in *Radio Recombination Lines*, ed. P. A. Shaver (Dordrecht: Reidel), p. 3.
Sharpless, S. 1959, *Ap. J. Suppl.*, **4**, 257.
Wilson, T. L. 1980, in *Radio Recombination Lines*, ed. P. A. Shaver (Dordrecht: Reidel), p. 205.
Wilson, T. L., and Jäger, B. 1987, *Astr. Ap.*, **184**, 291.
Wink, J. E., Wilson, T. L., and Bieging, J. H. 1983, *Astr. Ap.*, **127**, 211.

WILLIAM C. ERICKSON: Astronomy Program, University of Maryland, College Park, MD 20742

NAMIR E. KASSIM: NRL-Code 4131K, Washington, DC 20375-5000

KURT W. WEILER: NRL-Code 4131, Washington, DC 20375-5000

THOMAS L. WILSON: MPIfR, Auf dem Hügel 69, D-5300 Bonn 1, West Germany